Wireless Sub-Cellular Sized Stimulators for Minimally Invasive Deep Brain Stimulation with High Spatiotemporal Resolution

by

Yubin Cai

B.S., University of California, Los Angeles (2017)
M.S., University of California, Los Angeles (2019)

Submitted to the Program in Media Arts and Sciences,
School of Architecture and Planning,
in partial fulfillment of the requirements for the degree of

Master of Science in Media Arts and Sciences

at the

MASSACHUSETTS INSTITUTE OF TECHNOLOGY

September 2022

Author .....
Program in Media Arts and Sciences,
School of Architecture and Planning,
Aug 19, 2022

Certified by .....
Deblina Sarkar
Assistant Professor
Thesis Supervisor

Accepted by .....
Tod Machover
Academic Head, Program in Media Arts and Sciences

Wireless Sub-Cellular Sized Stimulators for Minimally Invasive Deep Brain Stimulation with High Spatiotemporal Resolution

by

Yubin Cai

Submitted to the Program in Media Arts and Sciences,
School of Architecture and Planning,
on Aug 19, 2022, in partial fulfillment of the
requirements for the degree of
Master of Science in Media Arts and Sciences

Abstract

Deep brain stimulation (DBS) has become a mainstream treatment for motor disorders associated with neurodegenerative conditions such as Parkinson's disease (PD). The DBS device, often called the "pacemaker for the brain", utilizes surgically implanted leads with 4-8 contacts points into the targeting area. The implanted electrodes are then used to deliver high frequency (>85 Hz) electrical stimulation via a pulse generator. In properly selected patients, DBS is proven to be remarkably effective, alleviating motor symptoms that either do not fully respond to medication treatment (such as tremor) or are caused by it (levodopa-induced dyskinesia). However, current DBS technology comes with inherent limitations and problems, including: 1) the need of a large invasive foreign body (the electrode) which can cause lead infections, 2) low coverage of entire movement-related territory in the target nucleus, and 3) adverse side effects such as muscle twitches and sensory complaints caused by diffused current into the tissues.

In this work, we propose to develop a new paradigm of electrical neuromodulation, based on injectable micron-sized stimulator devices, which, once deployed, will allow tunable stimulation of the injected territory. The individual stimulators will produce highly localized stimulation effects, which will minimize current spread to neighboring structures. Since the stimulator devices will be activated from an super-low-frequency (SLF) external magnetic field source, the procedure would not require placement of permanent wired leads in the brain. Additionally, given that a lightweight low-power wearable coil array will power the stimulator devices, a continuous portable DBS treatment of Parkinson's disease will be unprecedentedly made possible.

Thesis Supervisor: Deblina Sarkar
Title: Assistant Professor

Wireless Sub-Cellular Sized Stimulators for Minimally Invasive Deep Brain Stimulation with High Spatiotemporal Resolution

by

Yubin Cai

This thesis has been reviewed and approved by the following committee members

Thesis Advisor .....

Deblina Sarkar, Ph.D.
Assistant Professor at MIT
Department of Media Arts and Sciences

Thesis Reader .....

Edward S. Boyden, Ph.D.
Professor at MIT
Departments of Brain and Cognitive Sciences, Media Arts and Sciences, and Biological Engineering

Thesis Reader .....

Hugh Herr, Ph.D.
Professor at MIT
Department of Media Arts and Sciences

Acknowledgments

Foremost, I would like to express my sincere gratitude to my advisor Professor Deblina Sarkar for the continuous support of my Master's study and research, for her patience, motivation, passion, and profound knowledge. Her guidance helped me in all the time of research and writing of this thesis.

Besides my advisor, I would like to thank the rest of my thesis committee: Professor Edward S. Boyden, and Professor Hugh Herr, for their encouragement, and insightful comments.

I thank my colleagues in the Nano-Cybernetic Biotrek Group at the MIT Media Lab: Benoit Desbiolles, Marta Airaghi, Baju Chiyezhath Joy, Shivam Kajale, Monochura Saha, Shubham Yadav and Jad Hanna for the inspiring discussions, for the sleepless nights we were working together before deadlines, and for all the fun we have had in the last two years.

I would also like to thank David Bono for all his help in developing a variety of my experimental setups and the staff members of MIT.Nano – Kurt Broderick, Jorg Scholvin, and Kristofor Payer for their constant help and feedback during the nano-fabrication processes.

Last but not least, I would like to thank my family and my girlfriend, for their unconditional love and support.

Contents

Chapter 1

Introduction

In the modern century, we have witnessed tremendous advancements and success in medical care, which enables human beings to live longer than ever. However, as a lot of neurodegenerative diseases are age-dependent, we are also facing an unprecedentedly large population who are suffering from these diseases, such as AD, PD, and dementia [1]. Neurodegenerative diseases have become a tremendous social and economic burden. According to WHO, around 55 million people have dementia; This number is expected to rise to 139 million by 2050 [2]. According to literature, This type of disease cost the US healthcare system 655 billion US dollars in 2020 [3]. The key problem is that there is currently no way to cure such diseases, but only ways to improve the symptoms. One outstanding example is deep brain stimulation (DBS). It has been clinically proven to be effective in improving the symptoms of some neurodegenerative diseases such as Parkinson's [4, 5, 6, 7]. Nevertheless, the current approach to DBS is far from being ideal. It requires extremely complicated and high-risk neurosurgical procedures that implant highly invasive wired electrodes deep into the human brain [8, 8, 9, 10, 11, 12, 13]. None of the existing new techniques is a truly viable alternative to conventional DBS methodology.

1.1 Non-invasive Brain Stimulation Modalities

Given the ease of use, non-invasive modalities have been popular in clinical trials. Even though these technologies such as transcranial magnetic stimulation (TMS) and transcranial direct current stimulation (tDCS) do not need any surgically implanted devices or electrodes, they have significant drawbacks. For instance, TMS requires a very large power to drive a pair of bulky heavy coils [14, 15]. Also, very critically these types of techniques do not possess the spatial resolution required to stimulate small targets (the-state-of-the-art spatial resolution is on the order of few millimeters), cannot access deep brain regions and are significantly less effective and efficient than conventional deep brain stimulation through implanted electrodes [16, 17, 18, 19, 20, 21].

1.2 Minimally Invasive Brain Stimulation

In prior literature, there are many attempts in solving the engineering problem of conducting deep brain stimulation wirelessly by employing basically a minimally invasive modality where the stimulators are injected into the brain and get remotely actuated by a wave of different physical properties. Overal, the types of waves that have been exploited for such biomedical applications include optical, acoustic, and radiofrequency (RF) electromagnetic waves. These technologies also face several fundamental challenges:

- Optical waves suffer from high absorption and scattering in brain tissue, so that wireless optical devices can only be used for stimulation of tissue elements close to the brain's surface [22, 23]. Similarly, acoustic waves poorly penetrate through the skull and devices that use acoustic waves have only been used to affect the peripheral nervous system [24]. The acoustic devices are also physically large in dimensions, as reported in the prior literature.

- Devices based on RF EM waves have fundamental limitations as the device size needs to be comparable to the EM wavelength, so that the devices are

power efficient when operated in the reactive near-field range. Miniaturization in device size requires the use of RF electromagnetic waves at very high frequencies (tens of GHz and up), wavelength of which is relatively small [25]. However, the waves at such frequencies have extremely poor tissue penetration.

- Another technology worth mentioning is the use of magnetic nanoparticles based on low frequency magnetic fields, involving thermal stimulation. The key problem with the technology is that it requires genetic modification and cannot be easily translated to application on humans [26, 27, 28].

1.3 Wireless Magneto-Electric Stimulators

In this work, we propose to inject wireless micron-sized stimulators deep into the brain and 1 or 2 such devices will be placed in close proximity per neuron. After we apply a low-frequency magnetic field, these devices can generate electric potential across the top and the bottom to stimulate the degenerated neurons, by leveraging a novel magneto-electric effect in the materials that we use. Fundamentally, a magnetic field will cause a magnetostrictive film to stretch, which is coupled to a piezoelectric film that in turn generates the electric potential.

There are several advantages of our proposed technology compared to the existing technologies. First and foremost, we achieve minimal invasiveness given the stimulators' size (on the order of tens of microns in diameter and half micron in thickness). Secondly, since the low-frequency magnetic wave can penetrate deep through the tissues and the skull, our stimulators can be placed very deep into the brain and get remotely actuated. Given the high transduction efficient between magnetic field and electric potential from our devices, the power usage for the external source is very minimal. Also, electrical stimulation is universally applicable to many types of neurons. Last but not least, we aim to scale this technology to distribute the stimulators across multiple regions of the brain to achieve multi-region stimulation.

1.4 Thesis Objectives

Given the scope of the project and the novelty of the idea, this thesis focuses on investigating the fundamental physics and the material principles behind the proposed technology. Preliminary experiments and results are demonstrated and discussed; whereas, further in-depth electrical experiments on micron sized devices and in-vitro/ in-vivo experimental validations will be continued in author's Ph.D. studies.

1.4.1 Multi-physics Simulation

To fully understand the physics behind the magnetoelectric effect, I have developed a multi-physics simulation model in COMSOL and CST. It incorporates magnetic, electric and mechanical properties of the magnetostrictive layer and the piezoelectric layer in our bilayer device. I was able to validate the resonance frequency of the structure, the mechanical mode of the operation, and the magnitude of the generated voltage with results reported in the prior literature [29, 30]. It guided our fabrication process for creating the optimized stimulator device structure. Also, I have designed and validated the equivalent circuit model of a magnetostrictive thin film's inductive coupling with a nearby transceiver coil, which is robust and versatile enough to provide valueable insight to the advantages of magnetoelectric devices over conventional electromagnetic antennas.

1.4.2 Material Characterization

To characterize the materials' properties, I have utilized a wide range of characterization tools. a vibrating sample magnetometer (VSM) is used to measure the magnetic hysteresis loop of a 500 nm thick magnetostrictive thin film to validate the coercivity and saturation magnetization of the material. X-ray diffraction (XRD) measurement and piezoresponse force microscopy (PFM) are used to validate the piezoelectricity of a 500 nm AlN thin film. I have built a custom mangetostriction measurement setup with relies on the mechanical deflection of a mangetoelectric cantilever. Also, I have build a custom probe station setup to measure the magnetoelectric coupling coeffi-

cient of the micron sized devices with minimum physical contact to ensure minimum mechanical clamping effect and a minimum electrical noise level.

1.4.3 Nano Fabrication Process

I have thus far designed and developed a nano-fabrication process that is reliable and scalable to full-wafer scale. Transitioning from sub-mm devices to micron devices was very challenging. Major hurdles we have managed to overcome include:

- Magnetostrictive film requires to have near-zero film stress during the sputter deposition. The gun power and vacuum level need to be fine tuned.
- Inductively Coupled Plasma Etching (ICP RIE), that is typically used to dry etch piezoelectric thin films, is not compatible with magnetic materials
- Mechanically suspended structures in prior literature is not possible to be scaled to micron sizes [29]
- Alignment of photoresist mask in convectional instruments (such as MLA 150 aligner instrument) is difficult for micron resolution
- The low aspect ratio between the device size and the photoresist thickness makes it difficult to maintain a good mask sidewall profile for dry etching
- Aluminum nitride (AlN) is not compatible with TMAH, which is common in most of the standard developers
- Wet etchant of AlN, phosphoric acid, is a strong acid and can laminate and contaminate photoresist and etch a few magnetostrictive materials

1.5 Thesis Organization

The rest of the thesis is organized in the following way:

Chapter 2 dives into the fundamental physics of magnetostriciton, piezoelectricity and magnetoelectric effects. Multi-physics simulation in COMSOL and CST are

discussed to show validation of the theorized device performance. Also, equivalent circuit model is derived to elicit the quality factor of the magnetostrictive thin film and its comparison with the conventional electromagnetic counterpart.

Chapter 3 details the nano-fabrication processes for making the devices required in this work. A number of optimization steps for the development of the fabrication processes are also further discussed in this chapter.

Methods used for the characterization of the material properties are demonstrated in chapter 4. Finally, the device-level experiments and results to validate the magnetoelectric performance of the fabricated devices are also presented in chapter 4.

Chapter 2

Theory

2.1 Magnetostriction

Magnetostriction characterizes the property of a ferromagnetic material to either expand or contract upon the application of a magnetic field [32]. This occurs in two

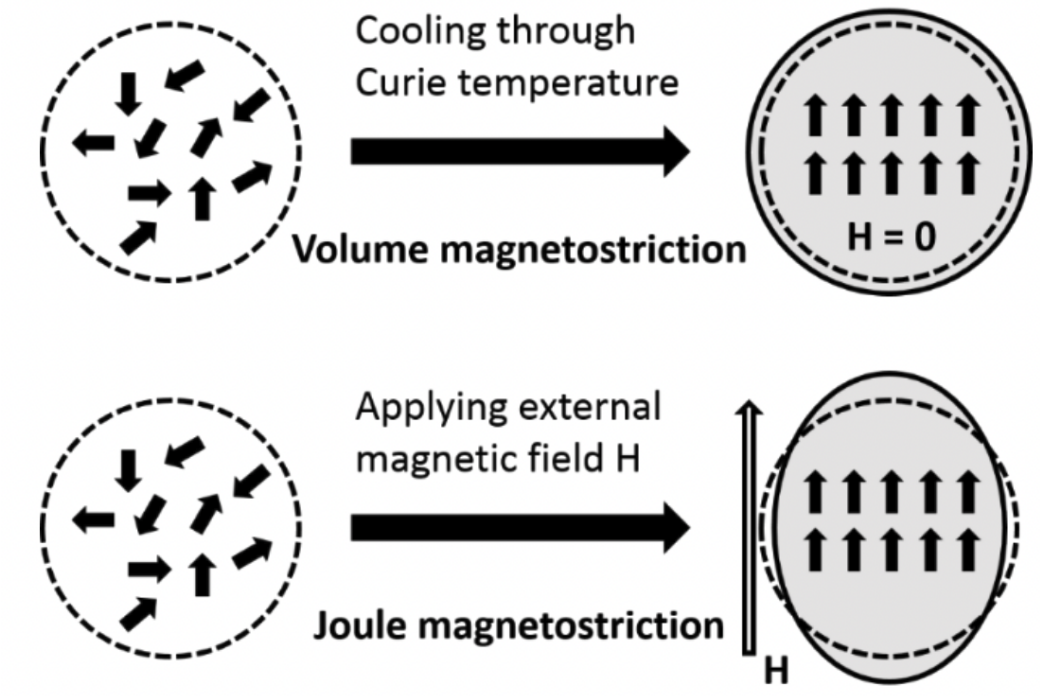

Figure 2-1: Demonstration of the effects of joule magnetostriction and Villari magnetostriction on a spherical object. Figure is cited from [31]

different ways: With volume magnetostriction, there is a uniform change in the shape in all spatial directions, which changes the volume. However, this effect is relatively small and can be neglected in most cases [33]. In contrast, Joule magnetostriction is more prominent, where there is a longitudinal change in the thin film along the applied field whereas the volume remains the same. As shown in Figure 2-1, the two different magnetostriction effects are illustrated. The change in length Δl in relation to its original length is called the magnetostriction coefficient λ [33],

$$\lambda = \frac{\Delta l}{t} \tag{2.1}$$

If there is an expansion along the magnetic field, λ a positive. This is called positive magnetostriction. For a contraction along the field, λ is negative and therefore there is a negative magnetostriction. The inverse effect, i.e. the magnetization caused by a change in shape, is called Villari magnetostriction. To characterize the magnetostriction coefficient of a material, a relatively easy and cost-effective way is to utilize the bending effect of a cantilever and deflection of laser beam [34, 35]. We can deposit/ attach magnetostrictive thin films onto non-magnetostrictive substrates and shape the thin films properly into a long cantilever. Due to the adhesion of the layer to the substrate, the cantilever will bend, instead of expanding or contracting. By determining the deflection D during the bending process, the magneto-elastic coupling b can be calculated according to the following equation[34],

$$b = \frac{1}{3}\frac{D}{l^2}\frac{E_s}{1+v_s}\frac{h_s^2}{h_f} \tag{2.2}$$

where l is the effective bending length, E_s is the young's modulus of the substrate, v_s is the Poisson's ratio of the substrate and h_s, h_f are the layer thicknesses of the substrate and the magnetostrictive thin film, respectively. The magnetostriction along one axis can then be calculated to be,

$$\lambda = b\frac{1+v_f}{E_f} \tag{2.3}$$

To calculate the total saturation magnetostriction, we can utilize the following relationship,

$$\frac{3}{2}\lambda_s = \lambda_{\parallel} - \lambda_{\perp} \tag{2.4}$$

2.2 Piezoelectricity

The piezoelectric effect describes the property of some ceramics and a few polymers to become electrically polarized when subjected to a mechanical force [36]. Only materials whose crystal structures do not have an inversion center show piezoelectric behavior. If a mechanical force is exerted on such a crystal, the crystal lattice is distorted and the ions in this lattice are shifted in relation to one another. As a result, dipoles form and polarization occurs. Conversely, if the material is polarized by an electric field, mechanical deformation occurs. This is called the inverse piezoelectric effect.

A measure of the strength of the piezoelectric effect is the piezoelectric coefficient d_{ij}. It describes the dielectric displacement D as a function of the applied mechanical stress σ in the case of the direct piezoelectric effect or the strain ϵ as a function of the applied electric field E for the inverse effect.

$$d_{ij} = (\frac{\partial D_i}{\partial \sigma_j})_E = (\frac{\partial \varepsilon_i}{\partial E_j})_\sigma \tag{2.5}$$

The dielectric displacement D is defined as the generated piezoelectric charge Q per area [37]. The indices i and j are the tonsorial components of the piezoelectric coefficient. In this work, the d_{31} is used. The first index indicates the direction of the elongation and the second the direction of the electric field. This means that the electric field and the strain generated are perpendicular to each other. The transverse effect is therefore present [38]. Various materials have already been investigated with regard to their use as a piezoelectric phase in thin-film composites for sensor technology [38, 39, 40, 41]. The focus of this work is on two piezoelectric materials: aluminum nitride (AlN) and Polyvinylidene fluoride (PVDF).

Aluminum nitride crystallizes in a hexagonal structure. As shown in Figure 2-

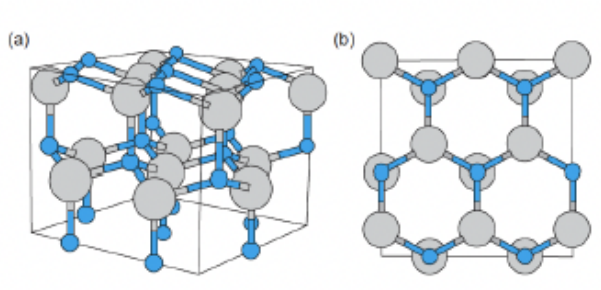

Figure 2-2: (a) The wurtzite structure of AlN. The Al atoms are shown in gray and the N atoms in blue. (b) Top view along the c-axis [42].

2, each aluminum atom is surrounded by four nitrogen atoms. A high piezoelectric effect is achieved by a strong c-axis orientation of the AlN structure, so a (002) orientation is preferable [42]. The production in the form of thin layers is done by reactive sputtering. When aluminum is atomized under a flow of nitrogen, the two components react to form aluminum nitride. While AlN has a comparatively low piezoelectric coefficient of $d_{31} = -3.5pm/V$ [40], it is characterized by its low dielectric losses, which makes it interesting for high-frequency applications [43]. On the other hand, PVDF is a piezoelectric polymer thin film, which is sold commercially in 30 um thick thin films. Bulk PVDF has very high reported piezoelectric coefficient of $d_{31} = -18pm/V$ a relative electric permittivity of 10. However, PVDF as a polymer is difficult to be deposited into very thin films (sub 1 um) with acceptable thickness uniformity.

2.3 Magnetoelectric Effects

The magnetoelectric (ME) effect is defined as the change in electric polarization caused by the application of an external magnetic field or vice versa as the change in magnetization caused by an electric field. Few single-phase materials exist that exhibit such behavior and show a comparatively small ME effect [28]. This problem can be overcome by using composites that consist of at least two different phases. Magnetoelectric composites were first presented by Van Suchtelen [29]. ME composites usually consist of piezoelectric and magnetostrictive materials that are mechanically

coupled to one another [30]. An external magnetic field generates a deformation of the magnetostrictive material, which is transferred to the piezoelectric material via the mechanical coupling. This deformation ensures polarization of the piezoelectric and leads to a measurable electric field. The principle described is expressed by the magnetoelectric voltage coefficient α_{ME}, which is a measure of the strength of the ME effect in a composite. This is given by

$$\alpha_{ME} = \frac{\partial \lambda}{\partial H} \frac{\partial \sigma}{\partial \lambda} \frac{\partial E}{\partial \sigma} \tag{2.6}$$

with λ as the magnetostriction caused by the magnetic field H, σ as the mechanical stress caused by the magnetostriction and E as the electric field caused by the mechanical stress. Since the deformation of the ME composites occurs in the form of vibrations, the ME coefficient can be increased many times over by using mechanical resonance effects [31].

Conventional electromagnetic (EM) antennas operate based on the principle of electromagnetic wave propagation from an electrical current flowing through a metallic conductor. One significant drawback of conventional EM antenna is that the size of the antenna needs to be comparable with one-tenth of the wavelength, otherwise the antenna is very inefficient in radiating outwards and harvesting energy [44, 45, 46, 47, 48]. Magnetoelectric antennas, however, relies on strain-mediated transfer from the incident electromagnetic wave into electrical polarization. The wavelength that magnetoelectric antennas radiation or energy harvesting relies on is not the EM wavelength but the acoustic wavelength. Since for a given frequency the acoustic wavelength in the magnetostrictive material is about five orders of magnitude smaller than the EM wavelength, sub-mm magnetostrictive antennas can be resonantly operated at low MHz frequencies [49].

2.4 Antenna Theories

Electrically small loop antennas are commonly used for electromagnetic field probing in the microwave frequency range and amateur radio in the HF (3 – 30 MHz) and

the VHF (30 – 300 MHz) bands [50]. A distinguishing feature of electrically small loops is that they are coupled to the magnetic field of the radio wave in the near-field region, as opposed to the electric field that dipoles are coupled to. More specifically, according to the Faraday's law of induction, the oscillating magnetic field of the incoming radio wave induces a current around the receiving loop antenna. This feature, along with their compactness, are the primary reasons why small loops are desirable for measuring the dielectric properties of a medium [51]. For example, in a 3-Tesla magnetic resonance imaging system, electrically small RF-coils are used to generate an oscillating and rotating magnetic field to excite the water protons within a human body, and to receive the reflected magnetic resonance (MR) signals [52]. Similarly, electrically small loop antennas are also the wining candidates for the transmitting and receiving antennas on the dielectric spectrometer used for underground water detection [53].

However, most electrically small antennas' sizes are on the order of tenth of wavelength, which prevents the usefulness of such an antenna at sub MHz. Biomedical implantable electromagnetic antennas based on RF EM waves have fundamental limitations as the antenna size gets too big to fit in any localized treatment/ diagnosis application. Miniaturization in device size requires the use of RF EM waves at very high frequencies which have low tissue penetration. Even though there are papers reporting antennas of tens of micron sizes, these antennas have very limited efficient RF transmitting/receiving range (on the order of few tens of microns) that make them barely useful in biomedical applications [54].

2.5 Multi-Physics Simulation

multi-physics simulations using COMSOL and CST have been conducted to guide our fabrication process for creating the optimized device structure.

For COMSOL simulations, We utilize the magnetostriction module, and the piezoelectricity module coupled through the mechanical strain transfer between the two layers. The magnetostrictive materials' parameters are obtained from the resonance

measurement of the centimeter-sized cantielvers; whereas the piezoelecric materials' parameters are based off the literature [29]. Figure 2-3 and Figure 2-4 show the simulation results of two difference device structures. Figure 2-3 is considering a circular structure with a nearly zero mechanical support. Figure 2-4 shows a resonator structure that has two sides anchored onto the substrate. We can see that the ideal case has a lot less noise spectrum than the drum structure does. Also, the z-axis mechanical displacement is dominant among the xyz axes, even though the field is only applied along the y axis, in-plane.

For the CST simulation, the magnetostrictive device's permeability profile is derived from an analytical MATLAB model. Figure 2-5 shows the schematic of the simulation interface. The device size considered is 500 um by 200 um by 28um. In simulation, the Q factor is much higher than what is seen in the measurement, which is expected when the sensor (a resonator) is present and the Rx coil is at the middle of the Tx coil, the coupling is not minimal (signified by a small valley in S12). It needs to be offset by a small distance to achieve minimal coupling.

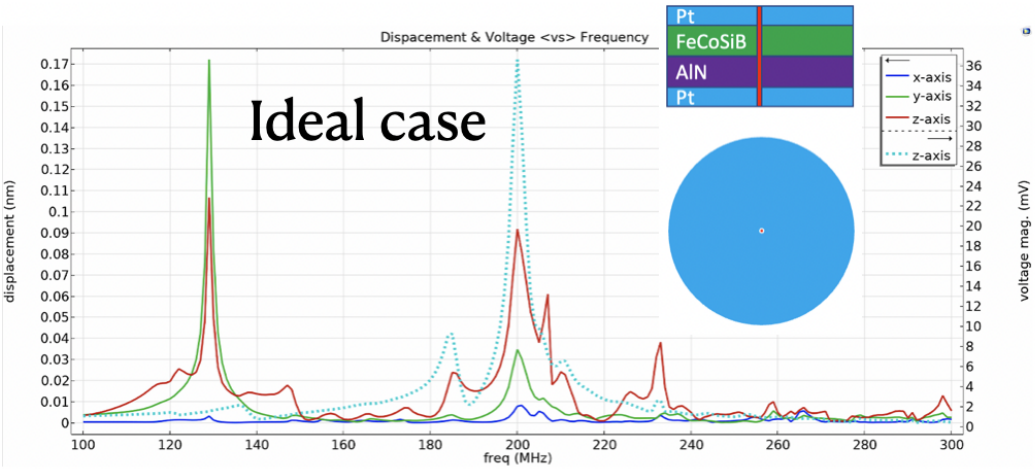

Figure 2-3: COMOSL simulation of a circular structure with nearly zero mechanical support. The device is under an in-plane magnetic field bias along the y-axis. The displacement on the left y-axis is that of the maximum displacement within the piezoelectric film. The voltage on the right y-axis is the electrical potential created by the top and the bottom electrodes of the piezoelectric AlN layer upon application of the incident magnetic field.

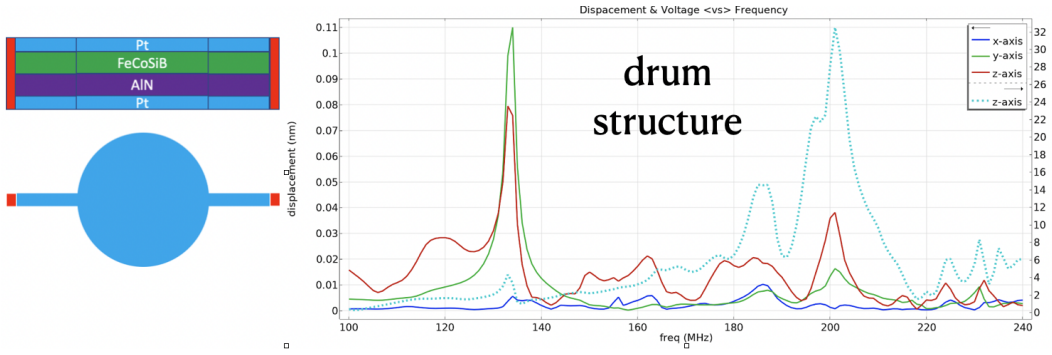

Figure 2-4: COMOSL simulation of a "drum" structure that has two ends anchored to the substrate while the middle is suspended in the air. The device is under an in-plane magnetic field bias along the y-axis. The displacement on the left y-axis is that of the maximum displacement within the piezoelectric film. The voltage on the right y-axis is the electrical potential created by the top and the bottom electrodes of the piezoelectric AlN layer upon application of the incident magnetic field.

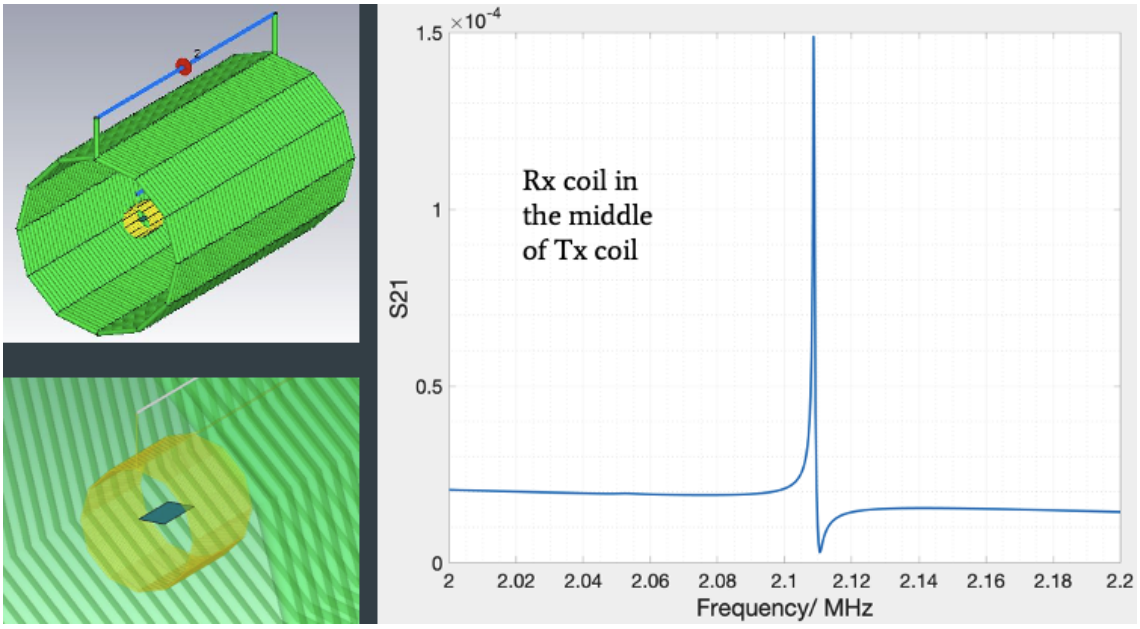

Figure 2-5: CST full-wave electroamgentic simulation of a magnetostrictive resonator. The permeability of the material is derived from an equivalent resonance model. The S21 data is acquired from the receiving coil.

Chapter 3

Nano-Fabrication

The fabrication process of the proposed micron sized devices requires a wide range of specialized techniques that are detailed in the follow subsections. Centimeter and millimeter devices are also fabricated to validate the quality of the deposited films and the results of the simulation.

3.1 Magnetron Deposition

Magnetron Sputtering is one of the methods of physical vapor deposition (PVD) and is used to produce a variety of thin layers of materials and alloys in the range from a few nanometers to several micrometers. The deposition takes place in an evacuated chamber. A non-reactive gas (usually argon) is introduced into the vacuum chamber and ionized in a strong electric field, forming a plasma of positive argon ions and electrons [**?**]. The argon ions are accelerated towards the cathode by the electric field. The material to be deposited, the target, is located there. The argon ions hit the target with high kinetic energy and knock out particles of the target material, which, due to the transferred residual energy, move in the direction of the substrate and are deposited there in the form of a thin layer. Magnetron sputtering is a modification of the traditional sputtering process in which permanent magnets are placed over the target. A bar magnet is placed in the center above the target and at the outer edge of the sample chuck. For depositing magnetostrictive and piezoelectric materials, it

is very crucial to control the vacuum pressure, gun power, background pressure and the deposition rate to ensure a suitable stress level in the as-deposited thin films to produce optimal piezomagnetic and piezoelectric coefficients respectively. The seed layer of the deposited piezoelectric material is also an important factor to affect the epitaxial growth of the material.

3.2 Annealing

Annealing of magnetic materials is a common technique in prior literature to increase the permeability of amorphous magnetic materials by eliminating edge domains caused by intrinsic stress [55]. For the magnetostrictive METGLAS thin film materials (28 um), the annealing is typically done by the manufacturer. Whereas, for the annealing of FeCoSiB, we need to anneal the samples after deposition, which can alter the film's stress level from compression to tensile as seen in prior literature. It is critical to heat the samples at a high enough magnetic field. We are using 2 kOe, which large enough to reinforce the shape anisotropy of the proposed magnetostrictive thin films in this work. The magnetic field is also crucial when the annealing chamber is cooled down.

3.3 Photo Lithography

Photo lithography process is one in which photoresist is spin coated across the wafer and patterned through light exposure at a certain wavelength and of a certain dosage. We are utilizing the maskless aligner (MLA) 150 tool at MIT.nano to pattern the wafer. Key parameters to tune include: pattern exposure precision, thickness, uniformity, side wall profile, developer chemistry and heat resistance. A successful photo lithgraphy process can ensure good subsequent dry etching qualities. Dosage test needs to be conducted for every material to ensure the resolution and the integrity of the patterned photoresist. Positive photoresist gets removed when shined by UV light, whereas a negatie photoresist gets hardened when shined. Developers are used

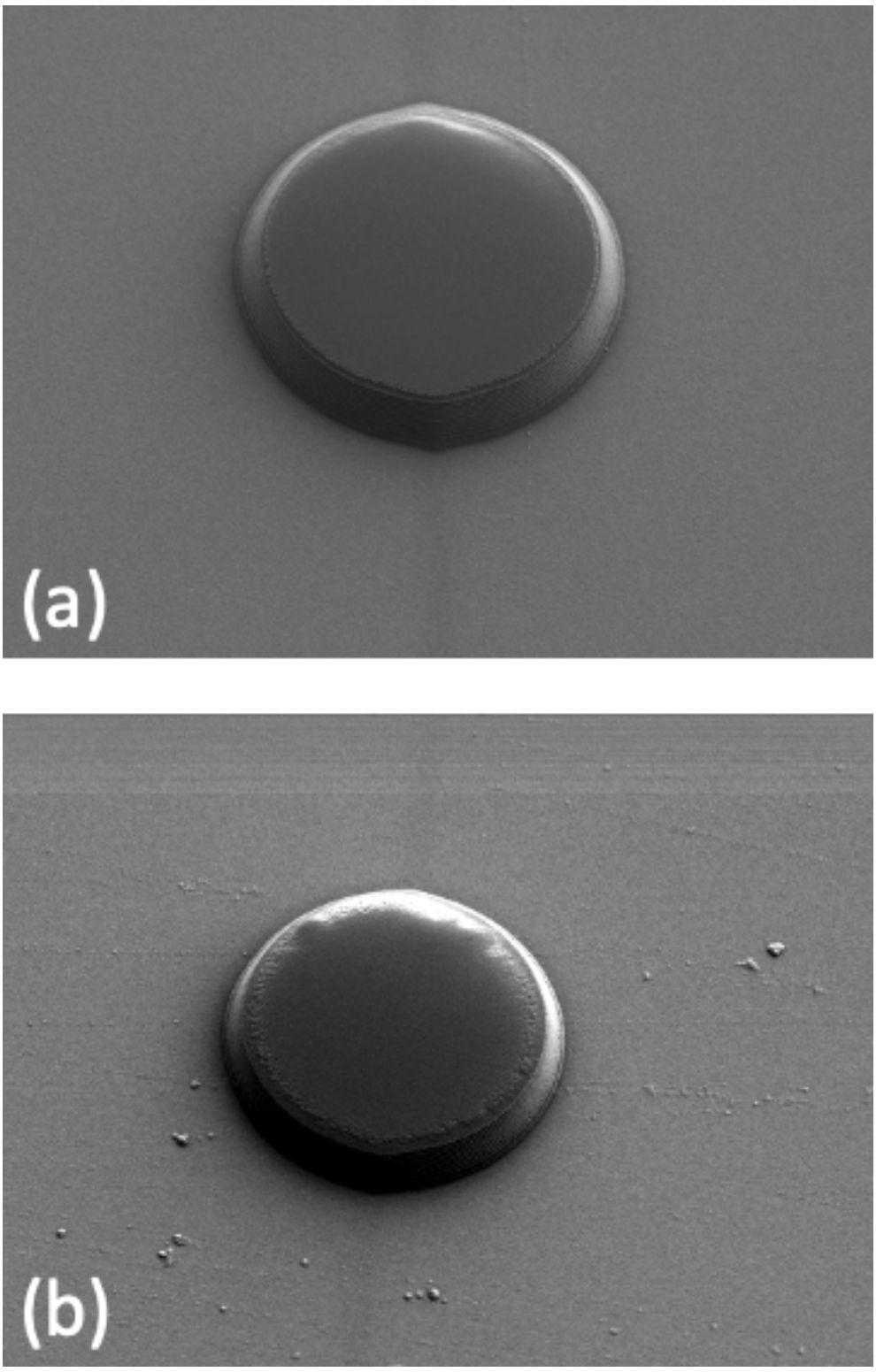

Figure 3-1: SEM images of photoresist fabricated for the ion-beam etching (IBE) processes. (a) without photoresist reflow, (b) with photoresist reflow.

after exposure to remove any unwanted photoresist. As shown in Figure 3-1, circular patterns are well developed on the positive photoresist. The size tolerance is about +/- 1 %, which is very reasonable. The reflow process ensures a skewed enough side wall profile of the photoresist to minimize redeposition in the subsequent dry etching process.

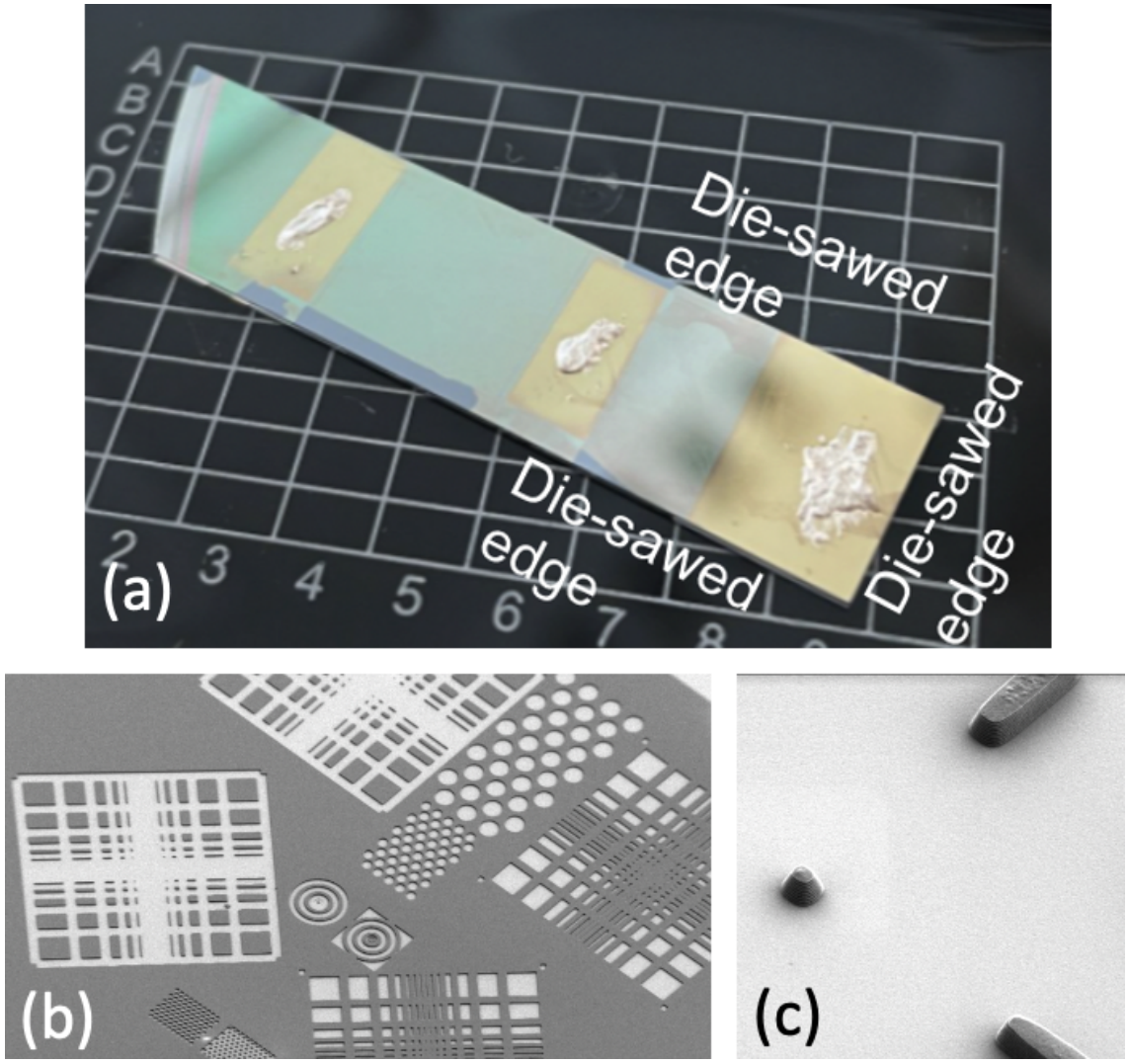

Figure 3-2: Demonstrations of the sample's prepared for the AlN shorting test. (a) Diesawed AlN samples, with the top gold layer deposition through a PDMS hard mask. (b) and (c) photoresist mask for lift off of the top gold layer deposition.

3.4 AlN Shorting Test

The piezoelectric material AlN is deposited through a sputter. Sputtering is a relative fast deposition method with a worse film uniformity than other deposition methods such as chemical vapor deposition (CVD). Sputter is typically used for manufacturing hundreds to thousands of nanometers; whereas, CVD is typicalled used for manufacturing few tens of nanometers. Early on in the project, one important task is to determine the electrical leakiness of the AlN material and characterize the electric permittivity/conductivity. Figure 3-2 lists some examples of the fabrication schemes to investigate the leakiness of the 500 nm thick AlN film. We have concluded the following:

- Diesawing through multiple metallic layers will likely short the layers electrically and should be avoided in the fabrication processes
- PDMS mask or metallic covering mask usually does not have a good enough adhesion to the substrate for lift off processes
- Conductive epoxy is consisted of nanoparticles that can penerate through holes in the thin films
- Photoresist mask should be used for depositing "islands" of the top electrodes and can prevent excessive shadowing effects of the sputter depositions
- Aluminum nitride (AlN) is not compatible with TMAH, which is common in most of the negative photoresist developers. So for the lift-off deposition processes on AlN, only positive photoresist can be used
- The AlN films that is deposited with 0.5 A/s deposition rate show very dense cross section that ensure a minimum electrical leakages with a relative electrical permittivity of around 6. This is consistent with the prior literature [29].

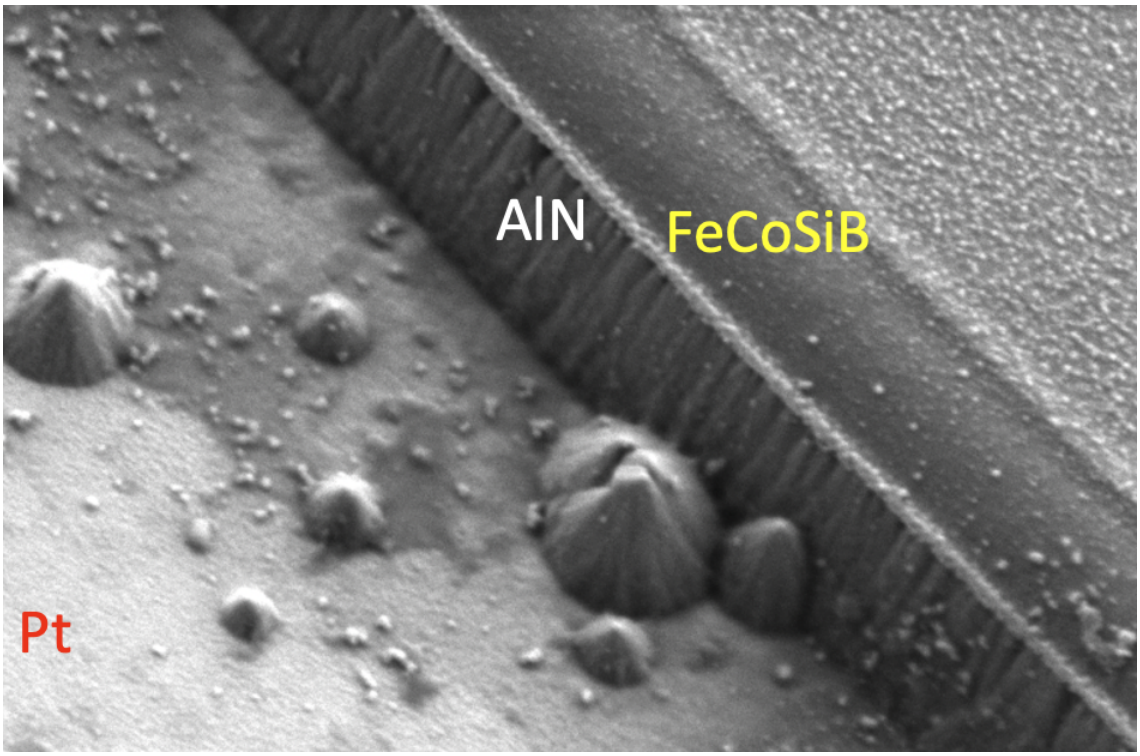

Figure 3-3: SEM images of photoresist fabricated for the ion-beam etching (IBE) processes. (a) without photoresist reflow, (b) with photoresist reflow.

3.5 Wet Etching of AlN

chemical etching is a method for removing material and is used primarily where high selectivity is required. This means that in the case of structures made of several different materials, if possible only one of them should be removed in the areas specified by the masking. Wet chemical etching processes typically have higher etch rates than dry etching methods. A disadvantage of wet-chemical etching is the high isotropy of this etching method [56]. As a result, effects such as undercutting occur, in which etching takes place under the masking and the quality of the desired structure is reduced. In the case of composites with AlN as the piezoelectric layer, the AlN is etched to expose the bottom platinum electrode and prevent die-sawing through the AlN layer for big device fabrications. In order to prevent undercutting, this is done in several steps. First, a positive photoresist is spin coated and patterned in MLA 150.

Then, a gold hard mask is deposited on top of the wafers, followed by lift off. Finally, the actual etching of the AlN with the hard mask as protection of the wanted area happens in phosphoric acid for approx. 40 minutes at 80 $°C$. The isotropic etching results in undercutting under the mask layer.

Shown in Figure 3-3 is an example of phosphoric etching AlN. The AlN shows a unique cross sectional structure that indicates <002> growth. The FeCoSiB on the top layer is contaminated by the phosphoric acid, which is a known effect. Therefore, in the process development, AlN needs to be pre-etched before the magnetostrictive material is deposited.

It is worthwhile to note that AlN is not compatible with strong acids such as TMAH. However, TMAH is often a constitute component in many photoresist developers, especially in all negative photoresist developers. Therefore, we can only use positive photoreists for the lift off processes on AlN. This can lead to dirty side wall and potential rip off of the top electrode layer.

3.6 Ion-Beam Etching (IBE)

Ion-beam etching (IBE) is a material removal technique and is one of the dry etching processes. Argon is first generated in a separate chamber by means of a voltage difference between two electrodes. The plasma ions are bundled by a coil and accelerated by a third electrode in the direction of the sample holder. However, before the ions hit the sample, the ion beam is neutralized. This is done using a highly heated wire from which electrons are emitted using a strong electric field, which then combine with the ions. To increase the etch rate, the beam strikes the sample at an acute angle. In addition, the sample is in constant rotation to ensure uniform etching. The great advantage of ion beam etching is the high anisotropy of this process, which means that there is no undercutting. However, it is also highly non-selective, which means that strict control of the etching time is necessary in order to prevent the photoresist from being removed or overheated.

As shown in Figure 3-4, the optimized IBE results are shown. There are no

visible re-depositions on the side walls of the devices and photoresist residuals on the cleaned devices. Each corresponding layer is easily differentiable by the different colors in SEM. The optimized parameters include: photoresist heating time, photoresist profile, photoresist reflow time, thicknesses, beam current, beam voltage, sample chuck vacuum, IBE etching rate, substrate rotating angles, scanning etch time and angles, and on/off time tables.

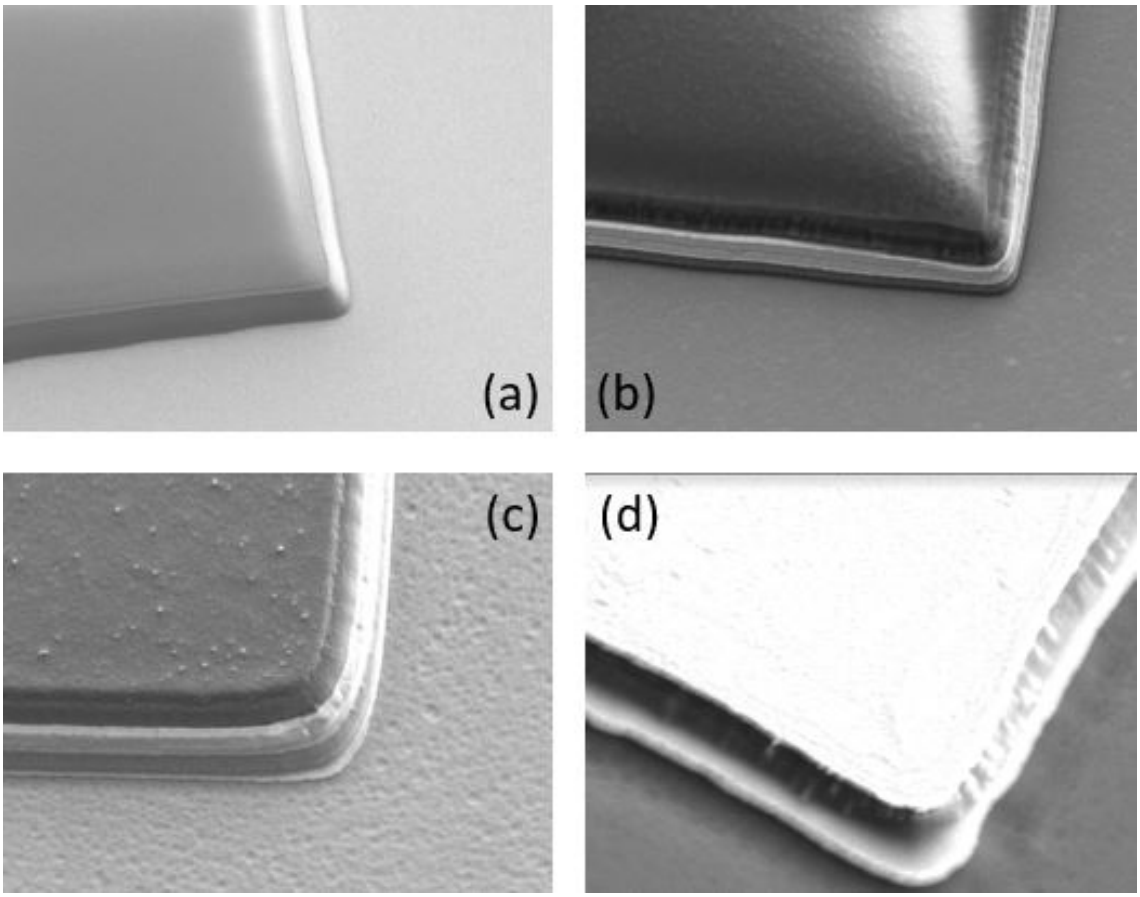

Figure 3-4: Scaning electron microscopy (SEM) images of the optimized ion-beam etching (IBE) processes results. (a) photoresist mask before dry etching. The side wall of the photoresist is very clean and smooth. (b) half way through an IBE process. (c) as-etched stack of materials. The bottom silicon substrate is exposed. (d) cleaned and optimized devices. This proves that the there is no significant photoresist mask residuals.

3.7 XeF2 Etch

XeF2 etch is a vapor etch technique that uses the selective etching of silicon by XeF2 vapors. It is a highly isotropic etch and typically has a much higher etch rate than wet etchants. We use XeF2 to release device stacks from the bottom silicon substrate. There are three different use scenarios for XeF2 etch in our process flow: 1) to release the device fully from the substrate for device retrieval and in-vitro experiments, (2) to make a structure for discs devices to have a pillar support underneath. This is for the ease of single-device characterization as the electrical contact is made through the landing of a probe onto the top electrode. (3) to make big suspended structure. XeF2 vapor has an etch rate that depends on the device size, vapor quantity and feature's aspect ratios. For precise control of the etch rate, a large sample size is required to ensure consistent release of devices. Full device release is done through submerging the chip in liquid and retrieved with iterative pipetting.

As sown in Figure 3-5, the devices are released from the substrate. However, the FeCoSiB layer's sidewall is also contaminated. This is because the silicon component in the FeCoSiB alloy gets etched very rapidly by XeF2 vapor. Therefore, a protection layer is used during the XeF2 etch and properly removed through oxygen asher afterwards in the final fabrication process. It is worthwhile to note that because of a small thermal contact to the bottom substrate with the wedge structure, removal of the photoresist at the end of the process is nontrivial. It requires a suitable pressure and plasma power to sufficiently clean the photoresist residuals on the layer surface.

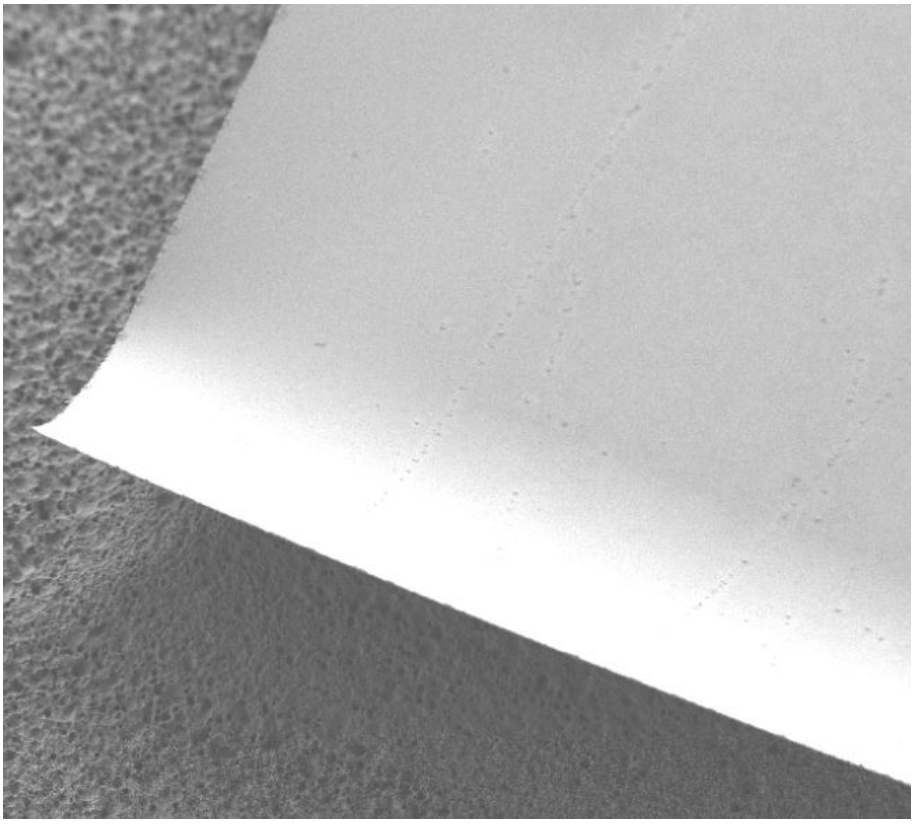

Figure 3-5: Scaning electron microscopy (SEM) half-suspended devices through XeF2 vapor etch. A curling effect is visible on the devices. This is because of the stress introduced in each layer during the sputtering process.

3.8 Centimeter and Millimeter Device Fabrications

To characterize the quality of the materials and validate the results from the multi-physics simulation, large centimeter and millimeter devices are also fabricated and tested.

The techniques for fabricating large devices are entirely different from those for micron device fabrications. First, pre-cut 5-mm-long by 2-mm-wide METGLAS films (magnetostrictive) are used along with PVDF (piezleoectric material). The bonding between the two materials are through conventional epoxy (Figure 3-6 (a)). To get an electrical contact from PVDF for the capacitve measurements, a thin 40 nm gold layer is sputter deposited. Then, the cantilever is mounted onto a 3D printed support (made by foamlab 3D printer in clear resin) with epoxy and bonded to the bottom custom PCB through soldering. Another fabrication strategy is also investigated as shown in Figure 3-6 (b). It uses a PVDF film (17-mm-long and 3-mm-wide) sandwiched between two top and bottom METGLAS films. Therefore, a gold deposition is no longer required as METGLAS is conductive. The 17-mm long cantilever is suspended in air and only physically soldered to the two wires for the voltage measurements.

Additionally, for nano-fabricated cantilevers it requires ICP etch to "shape" the AlN resonator, and wire bonding to create the electrical contact. Figure 3-7 shows a montage of devices fabricated through the fabrication processes developed with the tools at MIT.nano. It is made from 500nm FeCoSiB and 500 nm AlN sputter deposited blanket thin films.

Figure 3-6: Diagrams and images of the fabricated centimeter METGLAS/PVDF cantilevers. (a) a 5-mm-long cantilever made of gold/PVDF/Epoxy/METGLAS is bonded onto a 3D printed structure and a custom PCB. (b) a 17-mm-long cantilever is suspended in air and electric bonded to two 22 AWG wires for the top and the bottom METGLAS layers that serve as the electrodes.

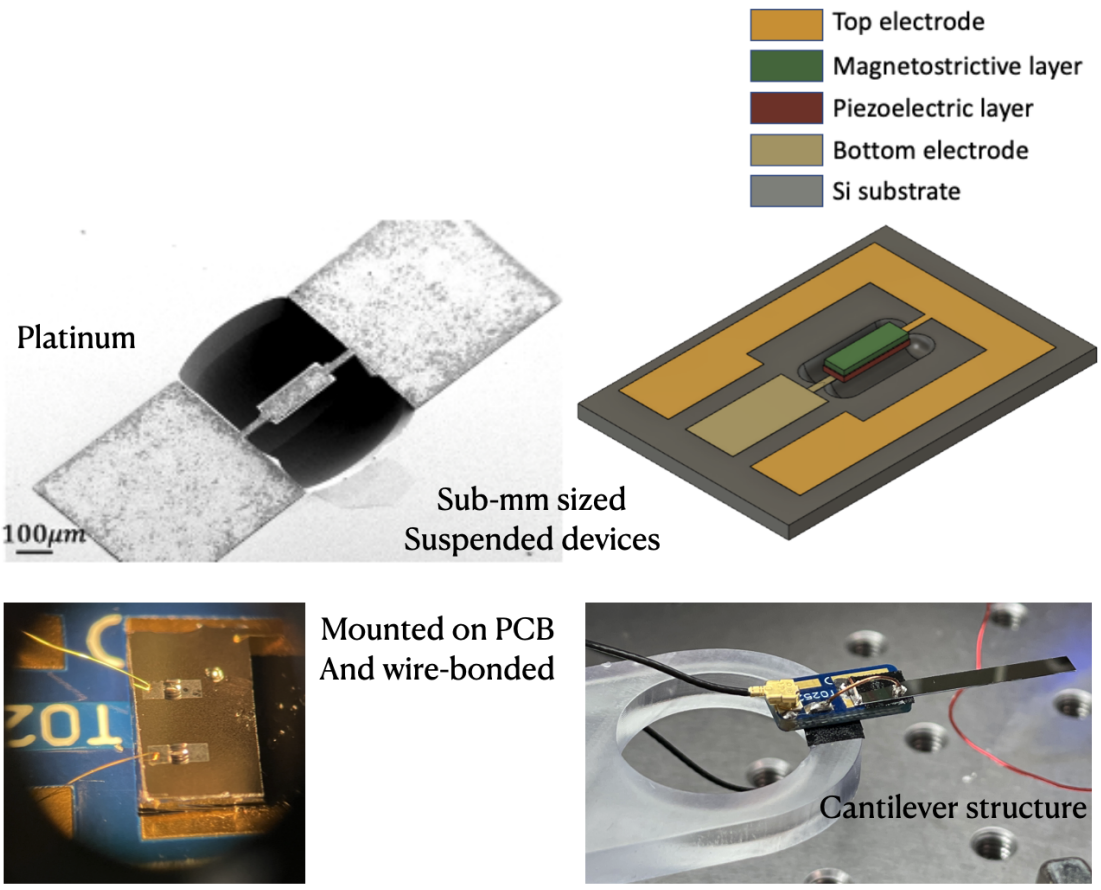

Figure 3-7: Diagrams and images of the fabricated centimeter cantilever and sub-millimeter devices.

Chapter 4

Material and Device Characterization

The magnetostrictive material and the piezoelectric material are characterized mainly by the magnetic hysteresis loop and the rocking curve measurement respectively. The material qualities were improved by optimizing the fabrication parameters. We have seem soft magnetism in the magnetostrictive FeCoSiB material and strong piezoelectricity in the pieozelectric AlN material. The main figure of merit for our devices is the magnetoelectric coupling coefficient, which is the transduction efficiency between the applied AC magnetic field and the generated electric voltage from the devices.

4.1 Vibrating Sample Magnetometer

Vibrating Sample Magnetometer (VSM) is an instrument that measures the magnetic hysteresis loop of a magnetic material based on the Faraday's Law of Induction. VSM typically has a pair of giant electromagnets, which generates a DC magnetic field that can align the magnetization in a sample along the direction of the applied field. Then, a piezoelectric crystal is attached to the end of the sample holder that vibrates the sample up and down rapidly. This leads to the magnetic dipole moment in the sample radiating an outgoing magnetic field that can be picked up from a receiving coil near the samples in the VSM. The current in the coil is proportional to the magnetization in the sample. Finally, a hysteresis loop is plotted out in the software with the applied field on the x-axis and the magnetization on the y-axis. Figure 4-1 shows

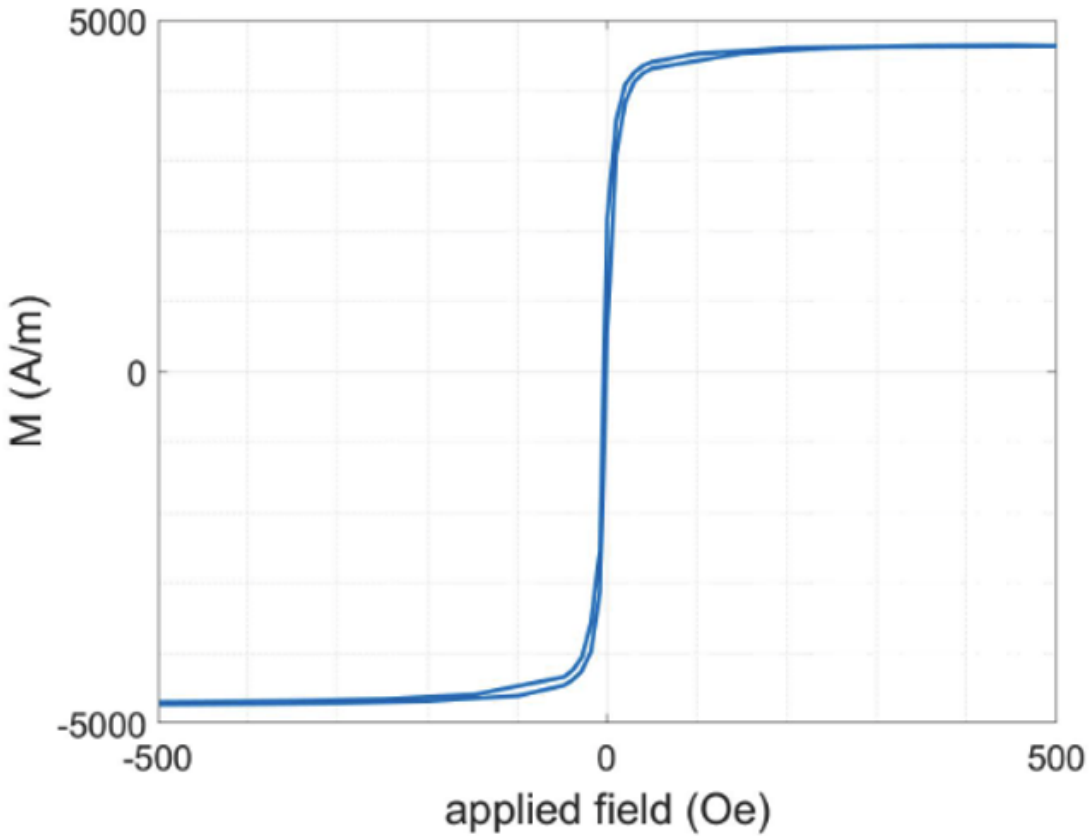

Figure 4-1: Measured hysteresis plot of 250 m thick FeCoSiB devices on AlN.

the measured hysteresis loop. We can see that the coercivity of the material is fairly low. This means that the material a very soft magnetic material and can be easily magnetized.

4.2 Magnetic Force Microscopy

Magnetic force microscopy (MFM) is a type of atomic force microscopy (AFM). MFM uses a magnetic tip that has an inherent magnetic moment, very close to the surface of the sample but not in contact. Any deflection of the tip caused by the magnetic sample underneath is measured through a position sensitive detector (PSD). The resolution of such deflection is conventionally on the order of few nanometers. Typically, the length of the cantilever that holds the tip is around 200 um long and the measured force from a magnetic sample is around 30 pN.

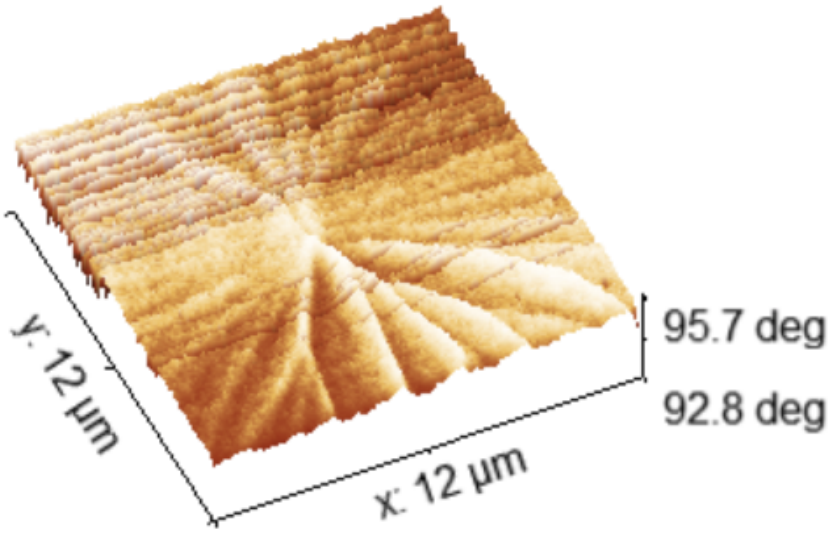

Figure 4-2: Measured phase of a 250 nm thick FeCoSiB material from magnetic force microscopy (MFM). The edge of the field-of-view is at the edge of the structures.

MFM only generates results of the surface magnetic properties and is often limited to the out-of-plane magnetization. This is because the tip that contains the magnetic moment is easy to be placed perpendicular to the plane of the sample, rather than in parallel. As seen in Figure 4-2, images of the out-of-plane magnetic domains are acquired on the AFM at the Harvard.CNS with the as-deposited 250 nm thick FeCoSiB devices. We can observe a radiant magnetic domain pattern that is mixed with some noise signals from the tip. We can spot the domains curved when they get to the edges of the magnetic material, which is consistent with our expectations. Further MFM experiments can validate the patterns obtained.

4.3 X-Ray Diffraction

X-ray diffractometry (XRD) is a method for determining the crystalline and chemical composition of materials using X-rays. To ensure a good <002> growth of the piezoelectric AlN material, it is important to measure a less than 3 degree full width half max (FWHM) value. The AlN's quality is also largely dependent on the bottom seed

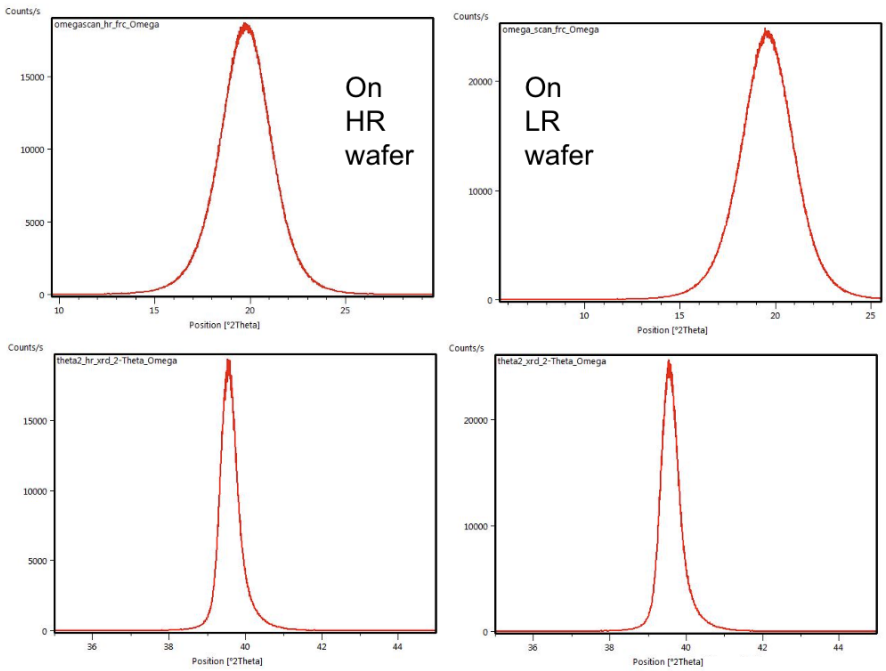

Figure 4-3: X-ray diffractometry (XRD) results of a 100 nm Pt seed layer for AlN depositions. The "HR" in the figure stands for high-resistivity and the "LR" stands for low-resistivity.

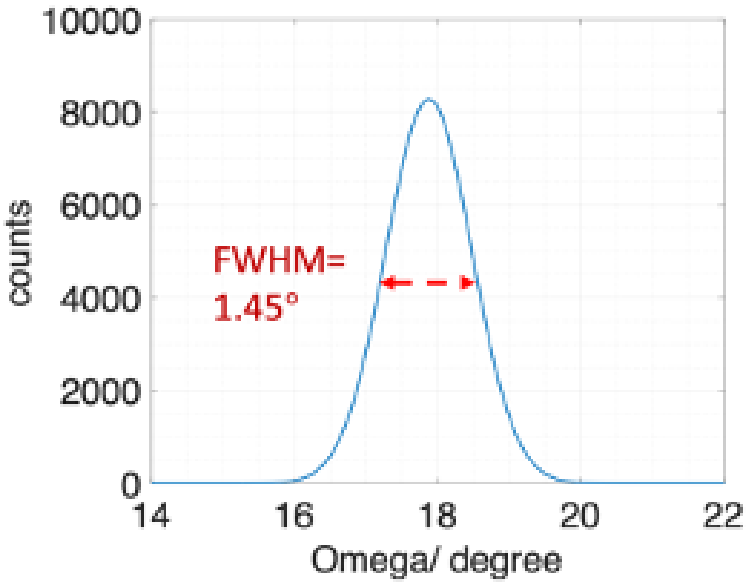

Figure 4-4: X-ray diffractometry (XRD) results of a 500 nm AlN.

platinum layer. We first measure the XRD results of different platinum materials, as shown in Figure 4-3. The results change slightly between the high-resistivity and the low-resistivity wafers but both are acceptable. We have processed the silicon sub-

strate with strong acid before depositing the platinum to ensure minimum substrate debris. The AlN deposition is carried out by the fabrication team at the Carnegie Melon University with their dedicated sputter for AlN. A high enough temperature is needed during the substrate heating to ensure a strong <002> growth in film. The stress in the film is also critical to ensure a large enough activity of the piezoelectricity. Further experiment with a four-point piezoelectricity measurement setup would be important to ensure a good piezoelectric coefficient.

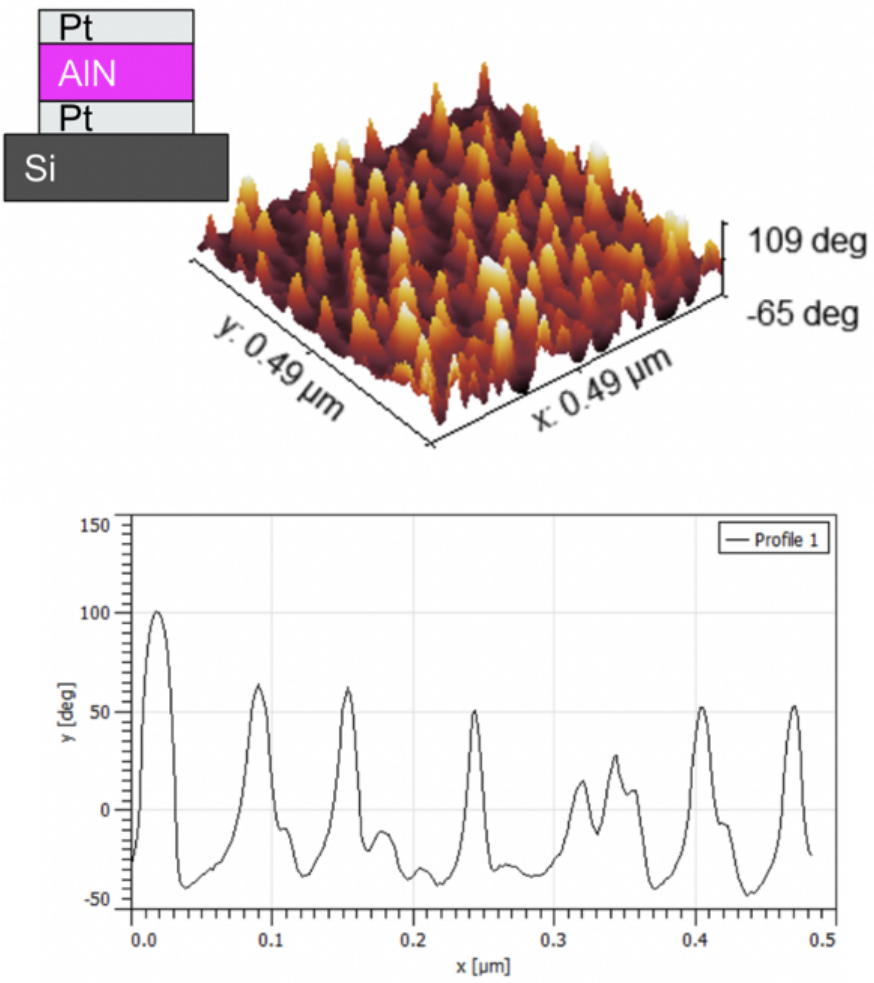

Figure 4-5: Measured phase of a 250 nm thick AlN from the piezoresponse force microscopy (PFM). The line plot shows a 2D curve of the data along the middle line in the field of view.

4.4 Piezoresponse Force Microscopy

Piezoresponse force microscopy (PFM) is a type of atomic force microscopy (AFM). PFM uses a conductive tip that gets in contact with the ferroelectric sample surface. It applies an alternating current at a particular frequency to the tip so that the sample is deformed through the piezoelectric effect. Consequently, the deflection of the tip is measured through a photodiode array.

Ass shown in Figure 4-5, from the phase image we can observe the piezoelectric domains across field of view in the sample. The domain sizes are consistent with the data reported in the prior literature [42]. It shows the piezoelectric activity of the AlN film, although the exact piezoelectric coupling coefficient is difficult to be determined from the PFM measurements. This should be done in a professional PE measurement setup such as the Aixacct Double-beam laser interferometry (DBLI).

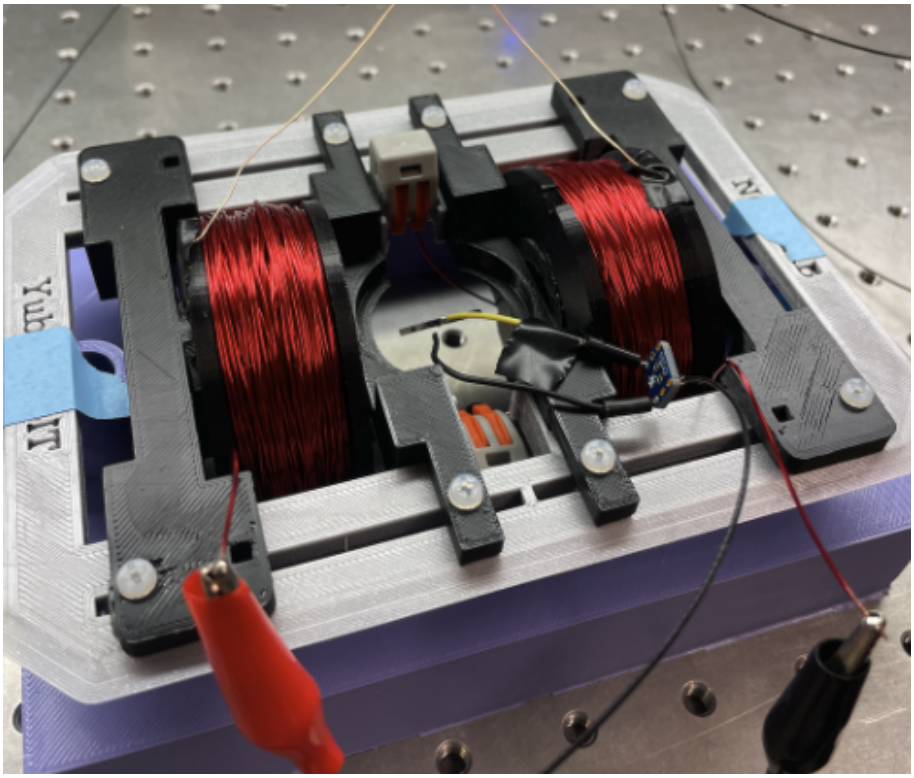

Figure 4-6: Measurement setup of a METGLAS PVDF magnetoelectric device. There are two sets of coils - a DC coil and a AC coil. The top and the bottom electrodes of the device are connected to a lock in amplifier directly.

4.5 Device Characterization

The fabricated devices have been measured on the bench. Centimeter devices are connected to a lock in amplifier to measure the generated voltages, when an AC coil is generating the AC excitation field. The current through the AC coil is also fed into the lock in amplifier as the reference signal. A DC bias field is required to align the magnetization of the magnetoelectric devices. Figure 4-6 shows the measurement setup that is used for the device characterization. Given that the centimeter devices are fairly large, the DC bias field is around 16 Oe. The DC bias field is inversely proportional to the dimension of the device. A resonance is measured in the magnetoelectric (ME) coupling coefficient with respect to the frequency (Figure 4-7). The maximum ME coupling coefficient is measured to be 25 V/(cm*Oe) at a resonant

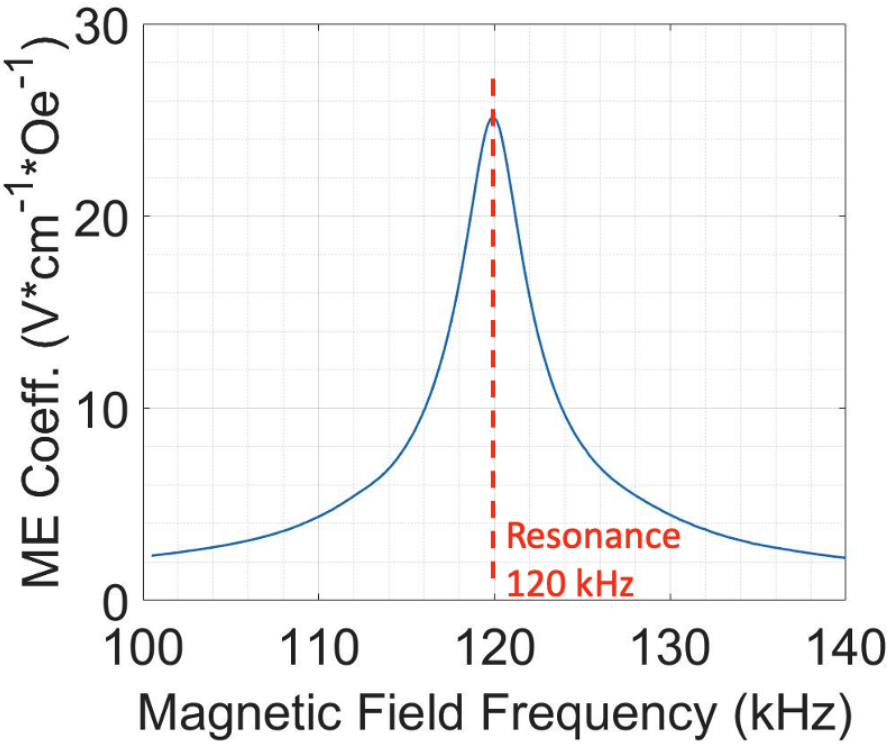

Figure 4-7: Measured magnetoelectric coupling coefficient of a 17-mm resonator device.

frequency of 120 kHz. The ME coefficient is defined to be the generated voltage per centimeter of the device along the field direction times the applied AC magnetic field. To demonstrate a modulation capability of the fabricated magnetoelectric devices, we have done amplitude modulated AC excitation field and observed a corresponding voltage waveform of the same amplitude modulation with a slight phase delay (Figure 4-8). Additionally, a 5-mm long cantilever made of METGLAS and PVDF from Figure 3-6 (a) is also measured. The resonance is also measured at around 4 kHz with a measured voltage of 50 uV (Figure 4-9). A cantilever structure has a lower mechanical resonant frequency than that of a structure in the same size suspended fully in the air.

On the other hand, micron device characterization requires a much more complicated process flow and dedicated custom setup to measure the voltage off the micron sized devices under a certain magnetic field. This method is under investigation right now and will be included in author's Ph.D. thesis.

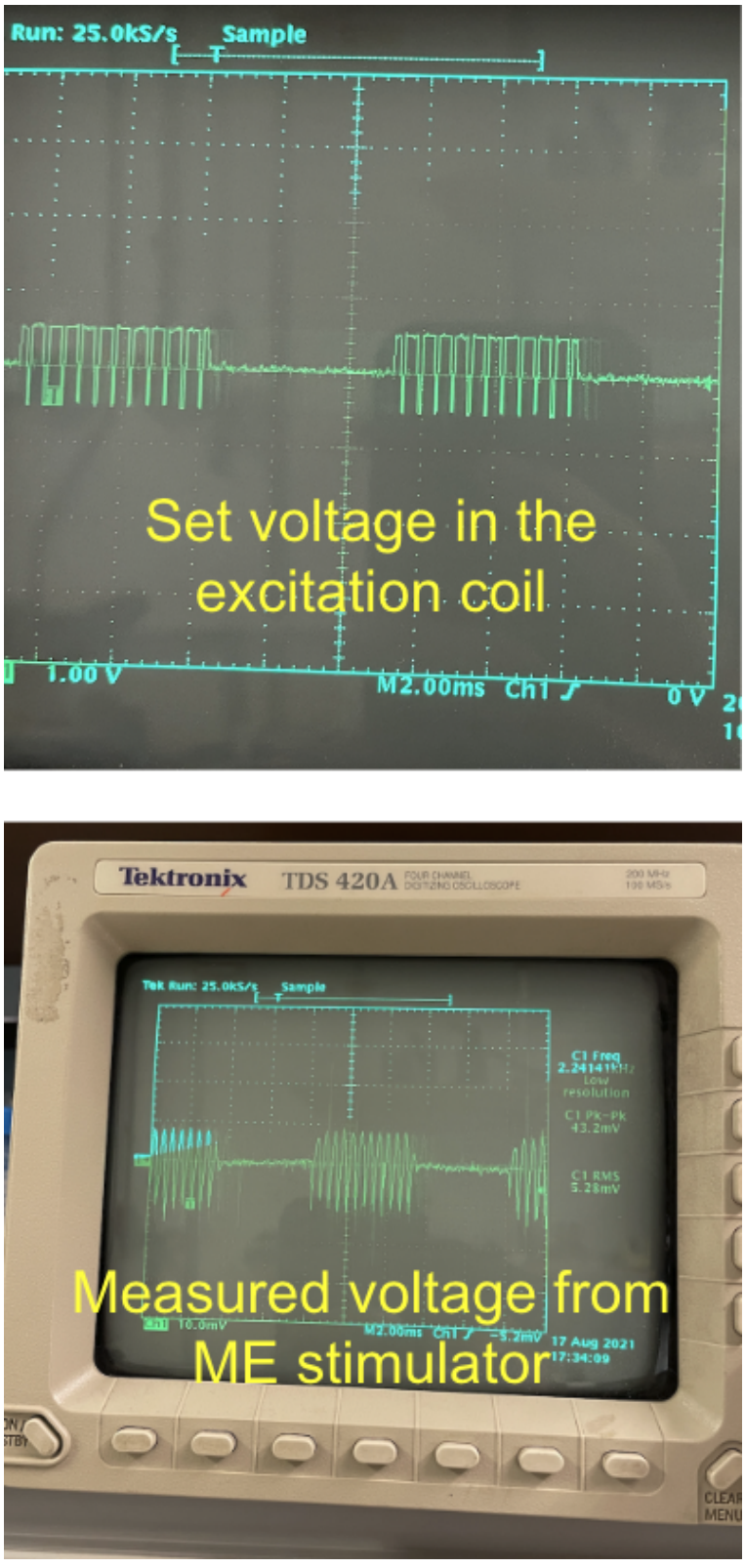

Figure 4-8: Measured voltages from the 17-mm resonator device under an amplitude modulated AC magnetic field.

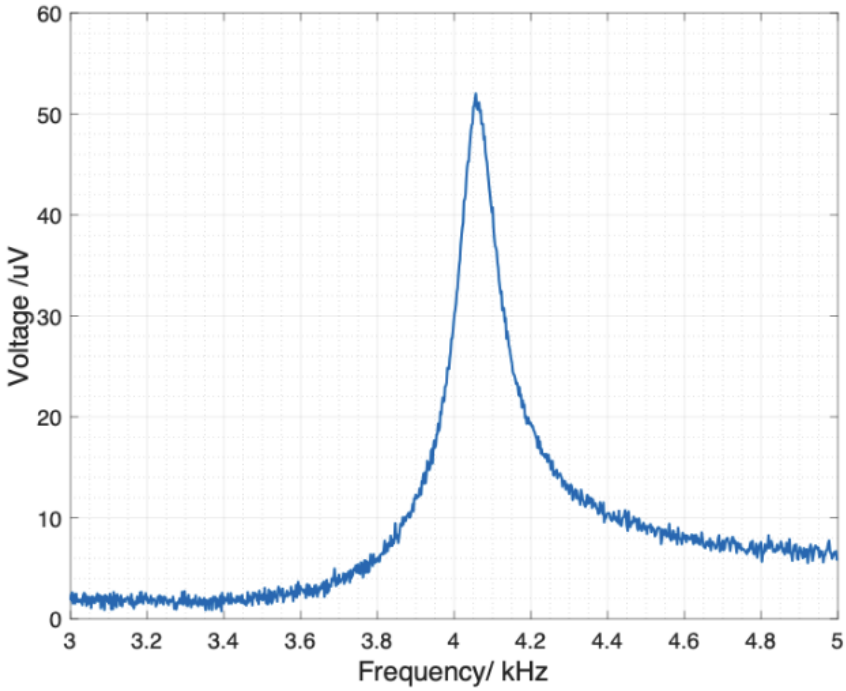

Figure 4-9: Measured voltage from a 5-mm magnetoelectric METGLAS PVDF cantilever.

Chapter 5

Discussions and Future Work

In this work I have investigated the physics principles of the magnetoelectric effects and how to design the device architecture to ensure good scalability and coupling efficiency. I have validated theorems through analytical modeling and multi-physics simulation. I have explored a variety of fabrication techniques of magnetoelectric devices from centimeter scale all the way to the micron scale. A number of interweaving challenges have been overcome, such as material compatibility and etching consistency, and a mature fabrication process has been developed. Additionally, materials have been individually characterized and validated through a wide range of characterization techniques of high precision. I have validated the magnetic properties, and the magnetostriction of the mangetostrictive material. The piezoelectricity and the piezoresponse of the piezoelectric material are also quantified. Finally, device-level experiments have been done on the large-scale centimeter sized and millimeter sized resonating devices. The optimal mechanical response in the frequency spectrum is thoroughly investigated with respect to an optimal magnetic field bias. Various custom experimental setups have been designed and buit from scratch.

Future work involves optimization of the micron devices' fabrication and strain measurement techniques. We have theorized that the stress in the as-deposited magnetostrictive films and the piezoelectric films are of utmost importance. The next step is to develop a strain measurement technique that can validate the piezomagnetic and the piezoelectric coefficients of the deposited thin films. This is a crucial

step especially for micron device manufacturing as the signal would be signficantly smaller than that of the large-scale devices. Also, once the devices are fabricated, the single-device characterization and bio-experiments will follow to further verify the magnetoelectric coupling efficiency in a biomedical medium. Challenges to overcome very small electric contact point on the micron devices and the necessity to mechanically suspend the devices to generate enough strain in the magnetostrictive thin film so that the piezoelectric layer can be effectively actuated. Future work will be continued into author's Ph.D. studies.

Bibliography

[1] Aaron D. Gitler, Paraminder Dhillon, and James Shorter. Neurodegenerative disease: models, mechanisms, and a new hope. *Disease Models & Mechanisms*, 10(5):499–502, may 2017.

[2] World Health Organization (WHO). World failing to address dementia challenge, 2021.

[3] Kenneth E. Thorpe, Allan I. Levey, and Jacob Thomas. U.S. Burden of Neurodegenerative Disease, 2021.

[4] T Wichmann and M R DeLong. Rationale for Surgical Interventions in Movement Disorders. In R H Winn, editor, *Youmans & Winn Neurological Surgery*, page in press. Saunders/Elsevier, Philadelphia, PA, 8th editio edition, 2020.

[5] T Wichmann, H Bergman, and M R DeLong. Basal ganglia, movement disorders and deep brain stimulation: advances made through non-human primate research. *J Neural Transm (Vienna)*, 125(3):419–430, 2018.

[6] C Wider, C Pollo, J Bloch, P R Burkhard, and F J Vingerhoets. Long-term outcome of 50 consecutive Parkinson's disease patients treated with subthalamic deep brain stimulation. *Parkinsonism Relat Disord*, 14(2):114–119, 2008.

[7] R A Esselink, R M de Bie, R J de Haan, M W Lenders, P C Nijssen, T van Laar, P R Schuurman, D A Bosch, and J D Speelman. Long-term superiority of subthalamic nucleus stimulation over pallidotomy in Parkinson disease. *Neurology*, 73(2):151–153, 2009.

[8] M I Hariz, S Rehncrona, N P Quinn, J D Speelman, C Wensing, and Group Multicentre Advanced Parkinson's Disease Deep Brain Stimulation. Multicenter study on deep brain stimulation in Parkinson's disease: an independent assessment of reported adverse events at 4 years. *Mov Disord*, 23(3):416–421, 2008.

[9] T A K Nguyen, M Djilas, A Nowacki, A Mercanzini, M Schupbach, P Renaud, and C Pollo. Analysis of patient-specific stimulation with segmented leads in the subthalamic nucleus. *PLoS One*, 14(6):e0217985, 2019.

[10] M Keane, S Deyo, A Abosch, J A Bajwa, and M D Johnson. Improved spatial targeting with directionally segmented deep brain stimulation leads for treating essential tremor. *J Neural Eng*, 9(4):46005, 2012.

[11] G A White-Dzuro, W Lake, I M Eli, and J S Neimat. Novel Approach to Securing Deep Brain Stimulation Leads: Technique and Analysis of Lead Migration, Breakage, and Surgical Infection. *Stereotact Funct Neurosurg*, 94(1):18–23, 2016.

[12] C Tolleson, J Stroh, J Ehrenfeld, J Neimat, P Konrad, and F Phibbs. The factors involved in deep brain stimulation infection: a large case series. *Stereotact Funct Neurosurg*, 92(4):227–233, 2014.

[13] M S Kim, J S Jeong, H S Ryu, S H Choi, and S J Chung. Infection related to deep brain stimulation in patients with Parkinson disease: Clinical characteristics and risk factors. *J Neurol Sci*, 383:135–141, 2017.

[14] Mark S George and Gary Aston-Jones. Noninvasive techniques for probing neurocircuitry and treating illness: vagus nerve stimulation (VNS), transcranial magnetic stimulation (TMS) and transcranial direct current stimulation (tDCS). *Neuropsychopharmacology*, (1):301–316, jan 2010.

[15] Marom Bikson, Pnina Grossman, Chris Thomas, Adantchede Louis Zannou, Jimmy Jiang, Tatheer Adnan, Antonios P. Mourdoukoutas, Greg Kronberg, Dennis Truong, Paulo Boggio, André R. Brunoni, Leigh Charvet, Felipe Fregni, Brita Fritsch, Bernadette Gillick, Roy H. Hamilton, Benjamin M. Hampstead, Ryan Jankord, Adam Kirton, Helena Knotkova, David Liebetanz, Anli Liu, Colleen Loo, Michael A. Nitsche, Janine Reis, Jessica D. Richardson, Alexander Rotenberg, Peter E. Turkeltaub, and Adam J. Woods. Safety of Transcranial Direct Current Stimulation: Evidence Based Update 2016. *Brain Stimulation*, 9(5):641–661, sep 2016.

[16] M S Kim, W H Chang, J W Cho, J Youn, Y K Kim, S W Kim, and Y H Kim. Efficacy of cumulative high-frequency rTMS on freezing of gait in Parkinson's disease. *Restor Neurol Neurosci*, 33(4):521–530, 2015.

[17] T Baumer, U Hidding, W Hamel, C Buhmann, C K Moll, C Gerloff, M Orth, H R Siebner, and A Munchau. Effects of DBS, premotor rTMS, and levodopa on motor function and silent period in advanced Parkinson's disease. *Mov Disord*, 24(5):672–676, 2009.

[18] O Arias-Carrion. Basic mechanisms of rTMS: Implications in Parkinson's disease. *Int Arch Med*, 1(1):2, 2008.

[19] E Formaggio, M Tonellato, A Antonini, L Castiglia, L Gallo, P Manganotti, S Masiero, and A Del Felice. Oscillatory EEG-TMS Reactivity in Parkinson Disease. *J Clin Neurophysiol*, 2021.

[20] O S Cohen, A Rigbi, G Yahalom, N Warman-Alaluf, Z Nitsan, A Zangen, and S Hassin-Baer. Repetitive Deep TMS for Parkinson Disease: A 3-Month Double-Blind, Randomized Sham-Controlled Study. *J Clin Neurophysiol*, 35(2):159–165, 2018.

[21] S Broeder, E Nackaerts, K Cuypers, R Meesen, G Verheyden, and A Nieuwboer. tDCS-Enhanced Consolidation of Writing Skills and Its Associations With Cortical Excitability in Parkinson Disease: A Pilot Study. *Neurorehabil Neural Repair*, 33(12):1050–1060, 2019.

[22] Yuanwen Jiang, Xiaojian Li, Bing Liu, Jaeseok Yi, Yin Fang, Fengyuan Shi, Xiang Gao, Edward Sudzilovsky, Ramya Parameswaran, Kelliann Koehler, Vishnu Nair, Jiping Yue, Kuang Hua Guo, Yin Fang, Hsiu Ming Tsai, George Freyermuth, Raymond C S Wong, Chien Min Kao, Chin Tu Chen, Alan W Nicholls, Xiaoyang Wu, Gordon M G Shepherd, and Bozhi Tian. Rational design of silicon structures for optically controlled multiscale biointerfaces. *Nature Biomedical Engineering*, 2(7):508–521, 2018.

[23] Kaylene C. Stocking, Alberto L. Vazquez, and Takashi D.Y. Kozai. Intracortical Neural Stimulation with Untethered, Ultrasmall Carbon Fiber Electrodes Mediated by the Photoelectric Effect. *IEEE Transactions on Biomedical Engineering*, 66(8):2402–2412, aug 2019.

[24] Benjamin C. Johnson, Konlin Shen, David Piech, M. Meraj Ghanbari, Ka Yiu Li, Ryan Neely, Jose M. Carmena, Michel M. Maharbiz, and Rikky Muller. StimDust: A 6.5mm3, wireless ultrasonic peripheral nerve stimulator with 82 In *2018 IEEE Custom Integrated Circuits Conference, CICC 2018*, pages 1–4. Institute of Electrical and Electronics Engineers Inc., may 2018.

[25] IEEE Standard for Safety Levels with Respect to Human Exposure to Radio Frequency Electromagnetic Fields, 3 kHz to 300 GHz. *IEEE Std C95.1-2005*, pages 1–238, 2006.

[26] Heng Huang, Savas Delikanli, Hao Zeng, Denise M. Ferkey, and Arnd Pralle. Remote control of ion channels and neurons through magnetic-field heating of nanoparticles. *Nature Nanotechnology*, 5(8):602–606, aug 2010.

[27] S. A. Stanley, J. E. Gagner, S. Damanpour, M. Yoshida, J. S. Dordick, and J. M. Friedman. Radio-Wave Heating of Iron Oxide Nanoparticles Can Regulate Plasma Glucose in Mice. *Science*, 336(6081):604–608, may 2012.

[28] Michael G. Christiansen, Alexander W. Senko, and Polina Anikeeva. Magnetic Strategies for Nervous System Control. *Annual Review of Neuroscience*, 42(1):271–293, jul 2019.

[29] Tianxiang Nan, Hwaider Lin, Yuan Gao, Alexei Matyushov, Guoliang Yu, Huaihao Chen, Neville Sun, Shengjun Wei, Zhiguang Wang, Menghui Li, Xinjun Wang, Amine Belkessam, Rongdi Guo, Brian Chen, James Zhou, Zhenyun Qian, Yu Hui, Matteo Rinaldi, Michael E. McConney, Brandon M. Howe, Zhongqiang Hu, John G. Jones, Gail J. Brown, and Nian Xiang Sun. Acoustically actuated ultra-compact NEMS magnetoelectric antennas. *Nature Communications*, 8(1):296, dec 2017.

[30] Amanda Singer, Shayok Dutta, Eric Lewis, Ziying Chen, Joshua C. Chen, Nishant Verma, Benjamin Avants, Ariel K. Feldman, John O'Malley, Michael Beierlein, Caleb Kemere, and Jacob T. Robinson. Magnetoelectric Materials for Miniature, Wireless Neural Stimulation at Therapeutic Frequencies. *Neuron*, 107(4):631–643.e5, aug 2020.

[31] Xianfeng Liang, Cunzheng Dong, Huaihao Chen, Jiawei Wang, Yuyi Wei, Mohsen Zaeimbashi, Yifan He, Alexei Matyushov, Changxing Sun, and Nianxiang Sun. A Review of Thin-Film Magnetoelastic Materials for Magnetoelectric Applications. *Sensors*, 20(5):1532, mar 2020.

[32] Robert C. O'Handley. *Modern Magnetic Materials: Principles and Applications*. Wiley Interscience, 1999.

[33] B. D. Cullity and C. D. Graham. *Introduction to Magnetic Materials*. Hoboken, New Jersey, 2nd edition, 2009.

[34] E. du Trémolet de Lacheisserie and J.C. Peuzin. Magnetostriction and internal stresses in thin films: the cantilever method revisited. *Journal of Magnetism and Magnetic Materials*, 136(1-2):189–196, sep 1994.

[35] D. Laumann, P. Hayes, C. Enzingmüller, I. Parchmann, and E. Quandt. Magnetostriction measurements with a low-cost magnetostrictive cantilever beam. *American Journal of Physics*, 88(6):448–455, jun 2020.

[36] Walter Heywang, Lubitz Karl, and Wersing Wolfram. *Piezoelectricity : evolution and future of a technology*. Berlin : Springer, 2008.

[37] B. Jaffe, W. Cook, and H. Jaffe. *Piezoelectric Ceramics*. Academic Press: New York, NY, USA, 1971.

[38] S. Trolier-McKinstry and P. Muralt. Thin Film Piezoelectrics for MEMS. *Journal of Electroceramics*, 12(1/2):7–17, jan 2004.

[39] Elena Aksel and Jacob L. Jones. Advances in Lead-Free Piezoelectric Materials for Sensors and Actuators. *Sensors*, 10(3):1935–1954, mar 2010.

[40] E. Yarar, V. Hrkac, C. Zamponi, A. Piorra, L. Kienle, and E. Quandt. Low temperature aluminum nitride thin films for sensory applications. *AIP Advances*, 6(7):075115, jul 2016.

[41] Gulnur Kalimuldina, Nursultan Turdakyn, Ingkar Abay, Alisher Medeubayev, Arailym Nurpeissova, Desmond Adair, and Zhumabay Bakenov. A Review of Piezoelectric PVDF Film by Electrospinning and Its Applications. *Sensors*, 20(18):5214, sep 2020.

[42] Stephan Marauska. *Highly sensitive micromechanical magnetoelectric magnetic field sensors*. PhD thesis, University of Kiel, 2013.

[43] Marc-Alexandre Dubois and Paul Muralt. Properties of aluminum nitride thin films for piezoelectric transducers and microwave filter applications. *Applied Physics Letters*, 74(20):3032–3034, may 1999.

[44] C. Rowell and E. Y. Lam. Mobile-Phone Antenna Design. *IEEE Antennas and Propagation Magazine*, 54(4):14–34, aug 2012.

[45] Robert C. Hansen and Robert E. Collin. *Small Antenna Handbook*. Wiley-IEEE Press, 2012.

[46] Constantine A. Balanis, editor. *Modern Antenna Handbook*. Wiley, aug 2008.

[47] M. Usami. An ultra small RFID chip: μ-chip. In *2004 IEE Radio Frequency Integrated Circuits (RFIC) Systems. Digest of Papers*, pages 241–244. IEEE.

[48] Xiaolin Hu, Kamal Aggarwal, Mimi X. Yang, Kokab B. Parizi, Xiaoqing Xu, Demir Akin, Ada S. Y. Poon, and H.-S. Philip Wong. Micrometer-Scale Magnetic-Resonance-Coupled Radio-Frequency Identification and Transceivers for Wireless Sensors in Cells. *Physical Review Applied*, 8(1):014031, jul 2017.

[49] Craig A. Grimes, Somnath C. Roy, Sanju Rani, and Qingyun Cai. Theory, Instrumentation and Applications of Magnetoelastic Resonance Sensors: A Review. *Sensors*, 11(3):2809–2844, mar 2011.

[50] Constantine A. Balanis. *Antenna theory: analysis and design*. Wiley, 2016.

[51] E.M. Cheng, M. F. Abdul Malek, S. F. Khor, K. Y. You, K.Y. Lee, M. A. Rojan, S. Abu Bakar, N. F. Mohd Nasir, Z. Zakaria, and W. H. Tan. reflection and dielectric measurement for salinity of water using microstrip loop antenna and dielectric probe. *International Journal of GEOMATE*, 11(24):2335–2340, 2016.

[52] Bernhard Gruber, Martijn Froeling, Tim Leiner, and Dennis W.J. Klomp. RF coils: A practical guide for nonphysicists: RF coils. *Journal of Magnetic Resonance Imaging*, 48(3):590–604, Sep. 2018.

[53] H. F. Morrison, A. Ratti, and E. Gasperikova. System and method for groundwater detection and evaluation, 2016.

[54] Mimi X. Yang, Xiaolin Hu, Demir Akin, Ada Poon, and H.-S Philip Wong. Intracellular detection and communication of a wireless chip in cell. *Scientific Reports*, 11(1):5967, dec 2021.

[55] P.T. Squire, D. Atkinson, and S. Atalay. Magnetostrictive and magnetoelastic properties of rapidly quenched wire. *IEEE Transactions on Magnetics*, 31(2):1239–1248, mar 1995.

[56] Marc J. Madou. *Fundamentals of Microfabrication*. CRC Press, oct 2018.